REGULAR ARTICLE

Kinetics and dynamics study of the H + CCl$_4$ → HCl(v', j') + CCl$_3$ reaction

J. Espinosa-García · C. Rangel · M. Monge-Palacios · J. C. Corchado

Abstract Based on a previous potential energy surface describing the H + CCl$_4$ reaction, a new analytical surface named PES-2010 was developed modifying both the functional form to give it more flexibility, and the calibration process in which exclusively theoretical information was used. Thus, the surface is completely symmetric with respect to the permutation of the four methane chlorine atoms, and no experimental information is used in the process. For the kinetics, the thermal rate constants were calculated using variational transition-state theory with semiclassical transmission coefficients over a wide temperature range, 300–2,500 K. The theoretical results reproduce the experimental variation with temperature. The influence of the tunneling factor is small, since the abstraction reaction involves the motion of a heavy particle (a chlorine atom) that cannot easily tunnel through the reaction barrier. The coupling between the reaction coordinate and the vibrational modes shows qualitatively that the HCl stretching mode in the products appears vibrationally excited. The dynamics study was performed using quasi-classical trajectory calculations, including corrections to avoid the zero-point energy problem. First, we found that the HCl(v', j') product mostly appears with small rotational energy and vibrational population inversion. Second, the state-specific scattering distributions show backward scattering, which becomes more noticeable as the HCl(v') vibrational state increases. Unfortunately, no experimental dynamics data are available for the title reaction, but the comparison with the kinematically similar and well-studied H + Cl$_2$ reaction shows good agreement, indicative of similar mechanisms. These kinetics and dynamics results seem to indicate that the potential energy surface is adequate to describe this reaction, and the reasonable agreement with experiment lends further confidence to this new surface.

Keywords Potential energy surface · Kinetics study · Dynamics study · H + CCl$_4$ light-heavy-heavy reaction

1 Introduction

In the same way that the H + Cl$_2$ system is a prototype of triatomic reactions with the light-heavy-heavy (LHH) mass combination, the H + CCl$_4$ system plays a similar role for gas-phase polyatomic reactions. These mass combinations are characterized by skew angles, β, close to $\pi/2$.

The construction of potential energy surfaces (PES) in polyatomic systems involves the evaluation of thousands of quantum chemical calculations, and hence a high computational cost, especially if chemical accuracy, ±1 kcal mol^{-1}, is needed. Obviously, this cost increases exponentially with molecule size and the number of electrons involved. If the complete construction of an analytical PES is usually far from trivial and is time-consuming, it is easy to understand that this problem is magnified in the case of the title reaction with its four heavy atoms. Due to these difficulties, in 2005, our group [1] constructed the first analytical PES for this reaction using an economical alternative based on an analytical PES for a similar reaction, introducing the appropriate modifications. We tested this PES-2005 against theoretical [2–5] and experimental

Published as part of the special issue celebrating theoretical and computational chemistry in Spain.

J. Espinosa-García (✉) · C. Rangel · M. Monge-Palacios · J. C. Corchado
Departamento de Química Física,
Universidad de Extremadura, 06071 Badajoz, Spain
e-mail: joaquin@unex.es

[2, 6] studies. First, the geometric, energy, and vibrational properties of reactants, products, and saddle point in general showed good agreement. The enthalpy of reaction at 0 K, −31.9 kcal mol^{-1}, agreed with the experimental value [6], −32.0 kcal mol^{-1}. Second, kinetically an extensive study using variational transition-state theory with semiclassical transmission coefficients over a wide temperature range, 300–2,500 K, was performed. We found that the PES-2005 reproduces the experimental forward rate constants [2], which were measured by Bryukov et al. using the discharge flow-resonance fluorescence technique, and proposed the following Arrhenius expression: k(T) = (1.36 ± 0.31) 0.10^{-10} exp(−2,927 ± 92 K/T) in cm^3 molecule^{-1} s^{-1}, in the temperature range 297–904 K, with an activation energy of 5.8 kcal mol^{-1}.

However, in spite of this agreement with theoretical and experimental data, the PES-2005 left some questions open: first, the planar or pyramidal geometry of the CCl$_3$ free radical, and second, the topology of the reaction path in the reactant and product zones. With respect to the first question, the planar or pyramidal structure of the CCl$_3$ product is still a debatable issue [6], although theoretical calculations [4, 5] obtain pyramidal geometries with a dihedral angle of about 145°. With respect to the second question, as was noted above, ab initio calculations of high level are prohibitive for this system, so that calculations have been limited to the density functional theory (DFT) level. Sheng et al. [4] performed DFT calculations finding a more pronounced drop in the product channel than those obtained with the PES-2005, with differences of 8–10 kcal mol^{-1} in the exit channel. This different depth will influence the dynamics of the reaction, for instance, in the product energy partitioning. To add more flexibility to the functional form of PES-2005, in the present work we include some modifications to that PES, constructing the PES-2010.

The article is organized as follows. In Sect. 2, electronic structure calculations are outlined, with especial attention paid to the barrier height information and the topology of the reaction path from reactants to products. In Sect. 3, a detailed description of the PES for the H + CCl$_4$ chlorine abstraction reaction is presented, highlighting the modifications introduced. The computational details are also

presented in this section. The kinetic results using variational transition-state theory with multidimensional tunneling effect are presented in Sect. 4, together with the dynamics results using quasi-classical trajectory (QCT) calculations. Section 5 is devoted to a comparison with the kinematically similar H + Cl$_2$ reaction. Finally, Sect. 6 presents the conclusions.

2 Electronic structure calculations: a review

One of the more difficult energy properties of a PES to estimate is the barrier height. Theoretical calculations have been reported by a few laboratories [2, 4, 5] for the title reaction using different levels—DFT or ab initio. The main results are summarized in Table 1. Depending on the level used (correlation energy and basis set), the barrier height (∆E) ranges from 5.1 to 6.0 kcal mol^{-1}, and the adiabatic barrier (∆Va, i.e., when the zero-point energy is included) ranges from 5.6 to 6.5 kcal mol^{-1}. Given that there is no direct experimental measurement for comparison (some authors compare the barrier height with the experimental activation energy, which is only a coarse approximation), it is not possible at present to take any value as reference in the subsequent calibration process (see Sect. 3). Given that the reaction is very exothermic [∆H$_R$(0 K) = −32.0 kcal mol^{-1}] [6], the transition state is early, i.e., it appears soon on the reaction path. As a consequence, the transition state is "reactant-like", and the length of the C–Cl′ bond that is broken is similar to its value in tetrachloromethane, while the Cl′–H bond formed is long. These distances also vary widely with the level used (Table 1).

Another important and computationally costly property is the topology of the reaction path from reactants to products. This has been calculated only by Sheng et al. [4] using the BHandHLYP/6-311G(d,p) DFT method, refining the energies at the PMP4/6-311 + G(3df,2p) single-point level. They obtained a deeper drop in the exit channel than those obtained with the PES-2005, which is typical of a very exothermic reaction.

In the present work, we have also performed DFT calculations using the MPWX model of Pu and Truhlar [7], where the percentage of Hartree–Fock (HF) exchange is X.

Table 1 Electronic structure calculations for the saddle point (energies in kcal mol^{-1}, and distances in Ångstrom units)

Method	∆E$^{\neq}$	∆Va^{a}	R(C–Cl′)	R(Cl′–H)	Ref.
UMP2/6-31G(d,p)	5.8	6.3	1.911	1.647	[2]
PMP4/6-311 + G(3df,2p)/BHandHLYP/6-311G(d,p)	6.0	6.5	1.899	1.810	[4]
CCSD(T)/6-311 ++ G(d,p)/MP2/6-311 ++ G(d,p)	5.1	5.6	1.907	1.654	[5]
MPW48	5.1	5.5	1.929	1.845	This work

^{a} Enthalpy at 0 K (i.e., including the zero-point energy)

The results are also included in Table 1, where the HF exchange is set to 48%. The saddle point presents a barrier height of 5.1 kcal mol^{-1} ($\Delta Va = 5.5$ kcal mol^{-1}), although the exothermicity is overestimated, -37.9 kcal mol^{-1}, relative to the experimental data [6], -32.0 kcal mol^{-1}.

In spite of the range of theoretical values, these will be the only data we use in the calibration of the new PES-2010 (see Sect. 3).

3 Potential energy surface and computational details

3.1 Potential energy surface

The analytical PES function we employ is the same as we used in our previous study [1], and therefore will not be repeated here. Basically, it consists of four London-Eyring-Polanyi (LEP) stretching terms, augmented by out-of-plane bending and valence bending terms. In order to better understand the modifications introduced, we shall start by outlining in some detail its mathematical form and terms.

The potential energy for a given geometry, V, is given by the sum of three terms: a stretching potential, V_{stretch}, a harmonic bending term, V_{harm}, and an anharmonic out-of-plane potential, V_{op},

$$V = V_{\text{stretch}} + V_{\text{harm}} + V_{\text{op}} \tag{1}$$

The stretching potential is the sum of four London-Eyring-Polanyi (LEP) terms [8], each one corresponding to a permutation of the four methane chlorines,

$$V_{\text{stretch}} = \sum_{i=1}^{4} V_3\left(R_{\text{CCl}_i}, R_{\text{CH}}, R_{\text{Cl}_i\text{H}}\right) \tag{2}$$

where R is the distance between the two subscript atoms, Cl_i stands for one of the four methane chlorines, and H is the attacking hydrogen atom, and where there are 12 fitting parameters, four for each of the three kinds of bond, R_{CCl_i}, R_{CH}, and $R_{\text{Cl}_i\text{H}}$. In particular, these are the singlet and triplet dissociation energies, D_{XY}^1 and D_{XY}^3, the equilibrium bond distance, R_{XY}^e, and the Morse parameter, α_{XY}, which depends on two switching parameters, a and b. Therefore, 14 parameters are required to describe the stretching potential.

One of the problems with this functional was that the equilibrium C–Cl distances for the reactants, saddle point, and products are the same, leading to a very rigid PES-2005. Based on a recent paper of Truhlar et al. [9] on the H + C$_2$H$_6$ reaction, in this paper a modification is included to endow the new surface with greater flexibility. The reference C–Cl bond distance is transformed smoothly from reactant to product using the equation,

$$R_{\text{CCl}}^0 = P_1 R_{\text{CCl,R}}^0 + (1 - P_1) R_{\text{CCl,P}}^0 \tag{3}$$

where P_1 is

$$P_1 = \prod_{i=1}^{4} T_1(R_{\text{CCl}_i}) \tag{4}$$

which is symmetric with respect to all the four chlorine atoms, and goes to zero as one of the chlorine atoms is abstracted, and T_1 is a geometry-dependent switching function, given by

$$T_1(R_{\text{CCl}_i}) = 1 - \tanh[w_1(R_{\text{CCl}_i} - w_2)] \tag{5}$$

where w_1 and w_2 are adjustable parameters. Therefore, this adds 2 new parameters (total 16 parameters) to describe the stretching potential.

The V_{harm} term is the sum of six harmonic terms, one for each bond angle in tetrachloromethane,

$$V_{\text{harm}} = \frac{1}{2} \sum_{i=1}^{3} \sum_{j=i+1}^{4} k_{ij}^0 k_i k_j \left(\theta_{ij} - \theta_{ij}^0\right)^2 \tag{6}$$

where k_{ij}^0 and k_i are force constants and θ_{ij}^0 are the reference angles. All these magnitudes are allowed to evolve from their value in tetrachloromethane to their value in trichloromethyl by means of switching functions. In total, 16 terms need to be fitted for the calibration of the V_{harm} potential.

The V_{op} potential is a quadratic-quartic term whose aim is to correctly describe the out-of-plane motion of trichloromethyl,

$$V_{\text{op}} = \sum_{i=1}^{4} f_{\Delta_i} \sum_{\substack{j=1 \\ j \neq i}}^{4} \left(\Delta_{ij}\right)^2 + \sum_{i=1}^{4} h_{\Delta_i} \sum_{\substack{j=1 \\ j \neq i}}^{4} \left(\Delta_{ij}\right)^4. \tag{7}$$

The general expressions are given by Jordan and Gilbert [10] and are not repeated here. The force constants, f_{Δ_i} and h_{Δ_i} are switching functions which are such that V_{op} vanishes at the tetrachloromethane limit, and Δ_{ij} is given by,

$$\Delta_{ij} = \cos^{-1}\left[\frac{(r_k - r_j) \times (r_l - r_j)}{\|(r_k - r_j) \times (r_l - r_j)\|} \cdot \frac{r_i}{\|r_i\|}\right] - \theta_{ij}^0 \tag{8}$$

where the vectors **r** are associated with the bonds R, and θ_{ij}^0 are the reference angles. The original expressions [10] were developed for the H + CH$_4$ reaction yielding the CH$_3$ radical, which is planar. However, there is some controversy about the geometry of the CCl$_3$ radical—whether it is planar or pyramidal [6]. Theoretical calculations [4, 5] at the DFT or ab initio levels give pyramidal geometries, with dihedral angles, ClCClCl, of about 145°. Therefore, in this paper we have modified the reference angle θ_{ij}^0 in Eqs. 6 and 8. Thus, the original expression [10],

$$\theta_{ij}^0 = \tau + (\tau - \pi/2)\left[S_\varphi(R_{CCl_i}).S_\varphi(R_{CCl_j}) - 1\right]$$
$$+ (\tau - 2\pi/3)[S_\vartheta(R_{CCl_k}).S_\vartheta(R_{CCl_l}) - 1] \qquad (9)$$

where $\tau = 109.4°$, and S_φ and S_θ are two switching functions, is replaced by

$$\theta_{ij}^0 = \tau + (\tau - \tau_1)\left[S_\varphi(R_{CCl_i}).S_\varphi(R_{CCl_j}) - 1\right]$$
$$+ (\tau - \tau_2)[S_\vartheta(R_{CCl_k}).S_\vartheta(R_{CCl_l}) - 1] \qquad (10)$$

where τ_2 is the bending angle ClCCl in the CCl_3 product, and τ_1 is related to τ_2 by the expression

$$\tau_1 = \pi - \arcsin\left[\frac{\sin(\tau_2/2)}{\sin(\pi/3)}\right] \qquad (11)$$

For the calibration of the V_{op} potential, 5 new parameters are needed.

The PES, therefore, depends on 37 parameters, 16 for the stretching, 16 for the harmonic term, and 5 for the out-of-plane potential. These 37 parameters give great flexibility to the PES, while keeping the VB-MM functional form physically intuitive.

Having selected the functional form, we next consider the calibration of the PES. This process has been described in detail elsewhere [1], so that here we shall present just a short description of the three steps of the process. Note, however, that, unlike the previous PES-2005 [1] which was calibrated against theoretical and experimental data, i.e., it was semiempiral in nature, in the present PES, denominated PES-2010, only theoretical information, DFT or ab initio, is used in the fitting procedure. In the first step, we change the parameters of the PES related to the geometric, energy, and vibrational properties of the reactants and products ($R_{CCl,R}^0$, $R_{CCl,P}^0$, R_{ClH}, R_{CH}, D_{CCl}^1, D_{ClH}^1, α_{ClH}), so that the geometries, heat of reaction, and vibrational frequencies agree with the available theoretical data. In the second step, we re-fit some parameters in order to reproduce the characteristics of the quantum mechanically calculated saddle point, in particular, the geometry, barrier height, and vibrational frequencies (D_{CCl}^3, D_{ClH}^3, D_{CH}^1, D_{CH}^3, α_{CH}). Finally, as the third step of the calibration, we re-fit some parameters of the analytical PES in order to reproduce the topology of the reaction, from reactants to products, using especially the switching functions. With this relation between parameters and reaction properties, we maintain the problem physically intuitive. Note, for instance, that the difference between D_{CCl}^1 and D_{ClH}^1, the dissociation energies of the broken and formed bonds, represents the energy of reaction, -34.92 kcal mol^{-1}. The final values of the parameters used in the fitting procedure are listed in Table 2.

Table 2 Parameters of the new PES

$R_{CCl,R}^0$	1.76000	Å
$R_{CCl,P}^0$	1.74000	Å
w_1	1.00	Dimensionless
w_2	1.76000	Å
R_{CH}	2.74000	Å
R_{ClH}	1.27460	Å
$D_{CCl_i}^1$	69.94900	Kcal mol^{-1}
D_{CH}^1	36.58000	Kcal mol^{-1}
D_{ClH}^1	104.86000	Kcal mol^{-1}
$D_{CCl_i}^3$	14.33400	Kcal mol^{-1}
D_{CH}^3	12.50300	Kcal mol^{-1}
D_{ClH}^3	25.52400	Kcal mol^{-1}
a_{CCl}	1.50000	Å^{-1}
b_{CCl}	0.14001	Å^{-1}
c_{CCl}	997.614	Å^{-1}
α_{CH}	0.73400	Å^{-1}
α_{ClH}	1.86770	Å^{-1}
k^{CCl_3}	1.15770	mdyne Å rad^{-4}
k^{CCl_4}	1.36470	mdyne Å rad^{-4}
aa_1	0.70095	Å^{-2}
aa_2	0.59996	Å^{-2}
aa_3	0.16595	Å^{-2}
aa_4	1.56998	Å^{-2}
A_θ	0.90787	Å^{-1}
B_θ	0.35488	Å^{-3}
C_θ	1.89155	Å
A_φ	2.40879	Å^{-1}
B_φ	0.20066	Å^{-3}
C_φ	1.92351	Å
$f_\Delta^{CCl_3}$	0.69575	mdyne Å rad^{-2}
$h_\Delta^{CCl_3}$	0.19150	mdyne Å rad^{-4}
α_3^s	0.14191	Å^{-3}
β_3^s	1.13383	Å
τ_2	2.04300	rad

3.2 Computational details

In the kinetics study, we used the variational transition-state theory (VTST) [11]. Starting from the saddle point geometry, we followed the reaction path toward both reactants and product, obtaining the minimum energy path, MEP [12], in the range $s = \pm 2.0$ bohr, s being the reaction coordinate. Along the MEP, we calculated vibrational frequencies after projecting out the motion along the reaction path using redundant internal coordinates [13, 14]. With this information, we calculated first the ground-state vibrationally adiabatic potential curve,

$$V_a^G(s) = V_{MEP}(s) + \varepsilon_{int}^G(s) \qquad (12)$$

where $V_{MEP}(s)$ is the classical energy along the MEP with its zero of energy at the reactants, and $\varepsilon_{int}^G(s)$ is the zero-point energy at s, and second the coupling terms [15], $B_{k,F}(s)$, measuring the coupling between the normal mode k and the motion along the reaction coordinate, mode F. These coupling terms are the components of the reaction path curvature, $\kappa(s)$, defined as

$$\kappa(s) = \left(\sum \left[B_{k,F}(s) \right]^2 \right)^{1/2} \qquad (13)$$

and they control the non-adiabatic flow of energy between these modes and the reaction coordinate [16, 17]. These coupling terms will allow us to calculate accurate semi-classical tunneling factors, and to give a qualitative explanation of the possible vibrational excitation of reactants and/or products, i.e., dynamical features, which are another sensitive test of the new surface.

Rate constants were estimated by using canonical variational transition-state theory (CVT) [11, 18]. Quantum effects in motions transversal to the reaction path were included by using quantum–mechanical vibrational partition functions in the harmonic approach, while quantum effects in the motion along the reaction path were included by using the microcanonical optimized multidimensional tunneling (μOMT) method, in which (at each energy) the transmission probability is taken as the maximum of two trial calculations, namely small-curvature tunneling (SCT) [19] and large-curvature tunneling (LCT) [20] methods. Recently, Truhlar et al. [21] have developed a new method to calculate the tunneling effect—the least-action tunneling transmission coefficient for polyatomic reactions, LAG—which is also tested in this paper. The rotational partition functions were calculated classically, and the vibrational modes were treated as quantum mechanical separable harmonic oscillators. All kinetics calculations were performed using the general polyatomic rate constants code POLYRATE [22].

In the dynamics study, we performed quasi-classical trajectory (QCT) calculations [23–25] using the VENUS96 code [26], customized to incorporate our analytical PESs. The accuracy of the trajectory was checked by the conservation of total energy and total angular momentum. The integration step was 0.01 fs, with an initial separation between the H atom and the tetrachloromethane center of mass of 6.0 Å, and a maximum value of the impact parameter of 3.0 Å. Since no experimental data are available, in this study we considered a relative translational energy of 15 kcal mol^{-1} and a tetrachloromethane rotational energy of 300 K. Batches of 100,000 trajectories were calculated, where the impact parameter, b, was sampled by

$$b = b_{max} R^{1/2} \qquad (14)$$

with R being a random number in the interval [0, 1]. The reaction probability, N_r/N_T, is the ratio of the number of reactive trajectories and the total number of trajectories, while the reaction cross-section is defined as

$$\sigma_r = \pi b_{max}^2 (N_r/N_T) \qquad (15)$$

A serious drawback of the QCT calculations is related to the question of how to handle the quantum mechanical zero-point energy (ZPE) problem in the classical mechanics simulation [27–37]. Many strategies have been proposed to correct for this quantum-dynamics effect (see, for instance, Refs. [27–31], and [34], and references therein), but no completely satisfactory alternatives have emerged. Here we employed a pragmatic solution, the so-called passive method [32], even knowing that this method perturbs the statistics, and therefore can lead to uncertainties in the dynamics study [38]. We used two approaches. The first discards all the reactive trajectories that lead to either the CCl_3 or the HCl product with a vibrational energy below their respective ZPEs. This we call histogram binning with double ZPE constraint, HB-DZPE. Schatz et al. [39, 40] showed that in atom + triatom reactions this approach yields unphysically small cross-sections, and they suggested that the ZPE constraint should be applied just to the newly formed bond. In the present case, it is applied only to the HCl product. This we call histogram binning with ZPE-HCl constraint, HB-ZPE-HCl. In this particular reaction, due to the small ZPE of both products, $CCl_3 = 4.76$ and $HCl = 4.33$ kcal mol^{-1}, the two approaches, HB-DZPE and HB-ZPE-HCl, give the same results, since the CCl_3 co-product is always obtained with energies above its ZPE.

The application of Eq. 15 requires the correct determination of the number of reactive trajectories, N_r, and the total number of trajectories, N_T, which are related to the previously analyzed ZPE problem. So, we have three possible values of N_r: counting (1) all the reactive trajectories, (2) only those that lead to both products with vibrational energy above their ZPE (HB-DZPE), and (3) only those that lead to HCl with vibrational energy above its ZPE (HB-ZPE-HCl). As we have just seen, these last two cases are equivalent for this particular reaction, so that the possible values reduce to two: counting all the reactive trajectories, and those with HB-DZPE. However, this form of removing trajectories from the N_r count without taking into account the behavior of the ensemble of trajectories can lead to erroneous results because it modifies the statistics [38]. Recently, Bonnet [41] proposed an adiabaticity correction in atom + diatom reactions which simply consists of omitting vibrationally adiabatic non-reactive trajectories in the calculations of final attributes. Based on

these ideas as applied to polyatomic systems, here we count the total number of trajectories in two ways. First, as has been usual in the QCT literature, we consider the total number of trajectories run in the calculation, in our case, $N_T = 100{,}000$. In the second approach, N_T in Eq. 15 is replaced by the total number of trajectories minus the number of reactive trajectories whose final vibrational energy is below the ZPE of the two products (HB-DZPE criterion), and minus the number of non-reactive trajectories whose final vibrational energy is below the ZPE of the CCl_4 reactant. This number is denoted $N_T{'}$. Therefore, we have four counting methods for the calculations of the reaction probability, (N_r/N_T), and therefore of the reaction cross-section, Eq. 15: N_r^{all}/N_T; $N_r^{HB-DZPE}/N_T$; $N_r^{all}/N_T{'}$; $N_r^{HB-DZPE}/N_T{'}$.

4 Results and discussion

4.1 Stationary points and reaction path

The properties for the final fit of the reactants and products are listed in Table 3, and those of the saddle point in Table 4. One observes in Table 3 that, in general, the agreement between PES-2010 and other theoretical values (DFT or ab initio) is good, indicating that the PES fit and functional form are very accurate. It is interesting to note that the C–Cl equilibrium distance varies along the reaction path, reproducing the theoretical and experimental behavior, and improving the behavior of the more rigid PES-2005, which wrongly assumed that the C-Cl equilibrium distance is constant over the entire surface. Moreover, the CCl_3 product presents a pyramidal structure, with a dihedral angle of 146.6°, reproducing the theoretical results. The harmonic vibrational frequencies are systematically lower than other theoretical values, but they reproduce the experimental data. However, because we looked for a balanced fit, the differences practically cancel out when we compute the vibrational zero-point energies and the changes in reaction enthalpy at 0 K. Thus, the latter is -32.1 kcal mol^{-1}, improving the agreement of other theoretical values with experiment [6], -32.0 kcal mol^{-1}.

The saddle point properties show reasonable agreement with the sparse ab initio and DFT quantum chemical calculations, although the new surface has a shorter C–Cl$'$ bond. The transition state is "early", i.e., it is a reactant-like transition state, where the length of the bond that is broken (C–Cl$'$) increases by only 3%, and the length of the bond that is formed (Cl$'$–H) is 53% larger than at the products. These results are similar to those obtained with the previous PES-2005, although the imaginary frequency characterizing this stationary point is closer to the theoretical values with the new surface. The combined effect of

potential energy and zero-point energy, i.e., $\Delta H_o^{\neq}$, the conventional transition-state enthalpy of activation at 0 K, 6.0 kcal mol^{-1}, is in good agreement with the values predicted by theoretical calculations.

As was noted above, one of the aims of the present work was to improve the topology of the reaction path from reactants to products of the earlier PES-2005, which presented a less pronounced drop than that indicated by theoretical results. Figure 1 plots the energy changes along the reaction path obtained with the new PES-2010, together with other theoretical values for comparison. These reproduce the theoretical results, markedly improving the topology of the previous PES-2005 in the exit channel.

Another important feature of the new PES-2010, related to the reaction path, is the description of the possible vibrational excitation in the entry and exit channels. The coupling terms, $B_{k,F}(s)$, between the reaction coordinate and the orthogonal bound modes control the non-adiabatic flow of energy between these modes and the reaction coordinate. Figure 2 shows their sum, κ, (Eq. 13) as a function of s. We found a weak coupling between the reaction coordinate and the C–Cl asymmetric stretch mode (762 cm^{-1}) in the entry channel, and a strong coupling of the reaction coordinate to the H–Cl stretching mode in the exit channel. Thus, this mode could appear vibrationally excited. These qualitative results agree with our previous PES-2005, and they will be analyzed in more detail below in the dynamics study.

4.2 Kinetics study

Table 5 lists the variational CVT/μOMT forward rate constants in the temperature range 300–2,500 K obtained with the PES-2010 surface, together with experimental [2] and other theoretical values [1, 4, 5] for comparison. Figure 3 shows the corresponding Arrhenius plot. The PES-2010 forward rate constants reproduce the experimental values in the common temperature range, which was already reproduced by the earlier PES-2005. In the latter, however, the experimental rate constants were used in the calibration process, and so the excellent agreement between theory and experiment in the common temperature range (300–900 K) simply represented a check of the consistency of the parametrization. In the PES-2010, however, only theoretical values were used in the calibration, and so the agreement with experiment reflects the accuracy of the new PES. Our results notably improve other theoretical values. Thus, the theoretical results of Sheng et al. [4] underestimate the experimental rate constants by factors of 2.8–1.7 in the common temperature range (300–900 K), and those of Louis et al. [5] overestimate them systematically by a factor of 2.5 (temperature range 700–2,500 K).

Table 3 Reactant and product properties

	CCl₄					CCl₃					HCl				
	PES10	Exp[a]	SLLXS[b]	LGS[c]	PES05	PES10	Exp[a]	SLLXS[b]	LGS[c]	PES05	PES10	Exp[a]	SLLXS[b]	LGS[c]	PES05
Geometry															
R(C–Cl)	1.760	1.760	1.771	1.772	1.760	1.740	1.740	1.712	1.714	1.760					
R(H–Cl)											1.275	1.275	1.276	1.273	1.275
α(ClCCl)	109.5	109.5	107.5	109.5	109.5	117.1	120	117.2	116.5	120					
η(ClCClCl)						146.6	180	≠180	143.6	180					
Frequency															
	762	776	814	819	809	844	898	933	934	827	2,969	2,890	3,046	3,087	3,025
	762	776	814	819	809	844	898	933	934	827					
	762	776	814	819	809	487	460	509	530	564					
	416	458	477	476	527	414	450	331	382	444					
	330	314	332	334	304	295	240	289	292	334					
	330	314	332	334	304	295	240	289	292	334					
	330	314	332	334	304										
	253	218	233	232	249										
	253	218	233	232	249										
Energy															
ΔH_f(0 K)	−32.1	−32.0	−28.9	−34.2[d]	−31.9										
ZPE	6.0	5.9	6.3	6.3	6.2	4.5	4.5	4.7	4.8	4.8	4.2	4.1	4.3	4.4	4.3

Geometries in Å and degrees, frequencies in cm⁻¹, energies in kcal mol⁻¹

[a] Experimental values from Ref. [6]

[b] SLLXS: first letters of authors from Ref. [4]. Values at the PMP4/BHHLYP level

[c] LGS: first letters of authors from Ref. [5]. Values at the CCSD(T)/UMP2 level

[d] Enthalpy of reaction at 298 K

Table 4 Saddle point properties

	PES-2010	SLLXS[a]	LGS[b]	MPW48[c]	PES-2005
Geometry					
R(C–Cl)	1.763	1.756	1.755	1.787	1.748
R(C–Cl′)	1.813	1.899	1.907	1.929	1.834
R(H–Cl′)	1.952	1.810	1.654	1.845	1.998
α(C–Cl′–H)	180	180	180	180	180
Frequency					
	784	838	842	814	826
	784	838	842	814	826
	719	747	837	719	754
	411	469	475	453	508
	323	320	323	306	318
	323	319	317	306	318
	314	319	317	305	283
	255	230	216	213	257
	255	230	216	213	257
	206	189	184	175	207
	206	189	184	175	207
	867 i	965 i	1,410 i	914 i	639 i
Energy					
$\Delta E^{\neq}$	5.4	6.0	5.1	5.1	5.2
$\Delta H^{\neq}$(0 K)	6.0	6.5	5.6	5.5	5.8
ZPE	6.5	6.7	6.8	6.4	6.8

Geometries in Å and degrees, frequencies in cm^{-1}, energies in kcal mol^{-1}

[a] PMP4/BHHLYP values from Ref. [4]

[b] CCSD(T)/UMP2 values from Ref. [5]

[c] This work

With respect to the tunneling effect (Table 5), the transmission coefficient, which mostly takes into account the quantum effects in the motion along the reaction path, increases the rate constants by small factors, 2.14–1.01 over the wide temperature range 300–2,500 K, similar to those found with the PES-2005. This behavior was to be expected, since the abstraction reaction involves the motion of a heavy particle (a chlorine atom) that cannot easily tunnel through the reaction barrier. We also tested large-curvature tunneling methods and found that the small-curvature tunneling paths are preferred in the μOMT method. The application of the newly developed LAG method [21] does not significantly change the rate constants (Table 5). This was to be expected, because tunneling is not as important as when lighter particles are involved.

The activation energy can be obtained by determining the slope of the Arrhenius plot. The values are 5.66 (300–400 K), 6.26 (300–900 K), and 6.96 (300–2,500 K) kcal mol^{-1}. In the common temperature range (300–900 K),
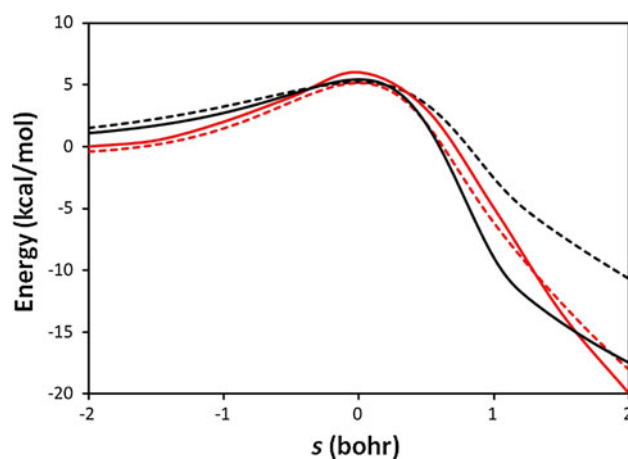
Fig. 1 Classical potential energy along the reaction path as a function of the reaction coordinate, *s*. *Black solid line*: analytical PES-2010 reaction path; *black dotted line*: analytical PES-2005; *red solid line*: PMP4/BHHLYP from Ref. [4]; *red dotted line*: MPW48 (present work)
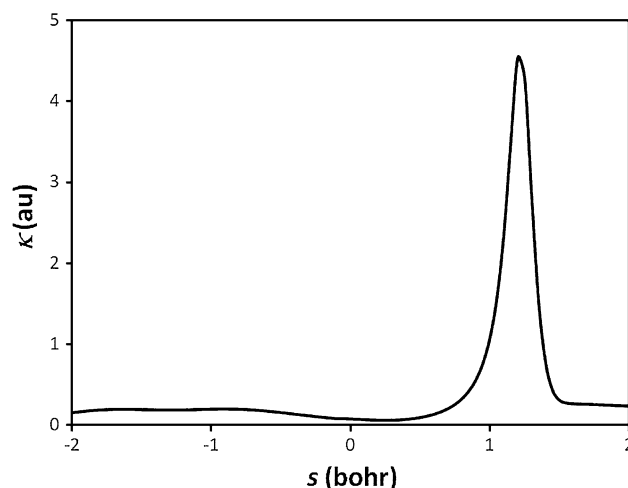
Fig. 2 Reaction path curvature, κ, as a function of reaction coordinate, *s*

our activation energy is close to the experimental value [2] of 5.8 ± 0.2 kcal mol^{-1}, and in agreement with the theoretical value reported by Sheng [4], 6.3 kcal mol^{-1}.

Finally, the equilibrium constants (K_{eq}) are calculated using only reactant and product properties, and hence it is a good test of the accuracy of their description. Table 6 lists the K_{eq} values in the temperature range 300–2,500 K together with the JANAF values [6] obtained from thermochemical calculations,

$$K_{eq} = \exp\left(-\frac{\Delta H_R^0}{RT} + \frac{\Delta S_R^0}{R}\right) \qquad (16)$$

where ΔH_R^o and ΔS_R^o are the enthalpy and the entropy of reaction, respectively. The PES-2010 reproduces the

Table 5 Forward rate constants (cm³ molecule⁻¹ s⁻¹) and transmission coefficients (κ) for the H + CCl₄ reaction

T (K)	PES-10[a]	Exp[b]	SLLXS[c]	LGS[d]	PES-05[e]	κ (μOMT)	κ (LAG)
300	6.79E−15	7.62E−15	2.94E−15		6.23E−15	2.14	2.03
350	2.56E−14	3.08E−14	1.14E−14		2.43E−14	1.73	1.67
400	7.29E−14	8.81E−14	3.21E−14		6.98E−14	1.51	1.47
500	3.41E−13	3.82E−13	1.45E−13		3.27E−13	1.30	1.27
600	1.01E−12	1.02E−12	4.15E−13		9.69E−13	1.20	1.18
700	2.31E−12	2.05E−12	9.10E−13	5.04E−12	2.18E−12	1.14	1.13
800	4.40E−12	3.46E−12	1.68E−12	9.26E−12	4.11E−12	1.10	1.09
900	7.42E−12	5.20E−12	2.77E−12	1.52E−11	6.86E−12	1.08	1.07
1,000	1.15E−11		4.19E−12	2.30E−11	1.05E−11	1.07	1.06
1,500	4.75E−11		1.65E−11	9.24E−11	4.18E−11	1.03	1.02
2,000	1.10E−10		3.70E−11	2.13E−10	9.21E−11	1.02	1.01
2,500	1.97E−10		6.46E−11	3.81E−10	1.56E−10	1.01	1.00

[a] CVT/μOMT values

[b] Ref. [2]

[c] CVT/SCT values, Ref. [4]

[d] TST/Wigner values, Ref. [5], k(T) = 2.6 × 10⁻¹⁵ T¹·⁶³² exp(−2,185/T), in the temperature range 700–2,500 K

[e] CVT/μOMT values on the PES-2005, Ref. [1]
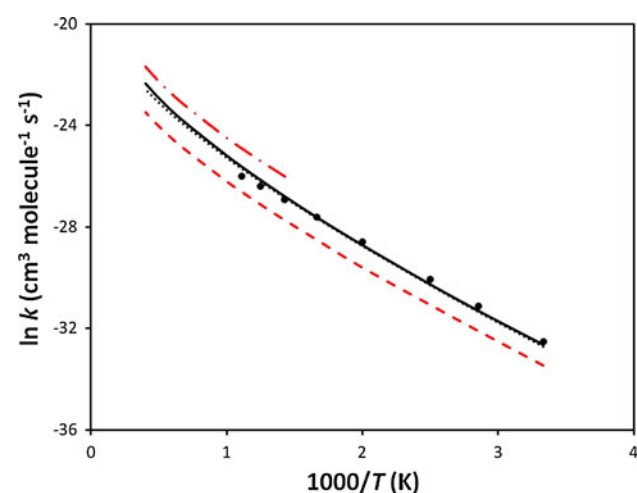
Fig. 3 Arrhenius plot of ln k (cm³ molecule⁻¹ s⁻¹) against the reciprocal of the temperature (K) in the range 300–900 K for the forward thermal reaction. *Black solid line*: PES-2010; *black dotted line*: PES 2005; *red dashed line*: theoretical values from Ref. [4]; *red dotted-dashed line*: theoretical values from Ref. [5]; *black circles*: experimental values from Ref. 2

Table 6 Equilibrium constants for the H + CCl₄ → HCl + CCl₃ reaction

T (K)	PES-10[a]	Exp[b]	PES-05[c]
300	3.82 E+26	3.72 E+26	2.97 E+26
350	1.63 E+23	1.62E+23	1.27 E+23
400	4.73 E+20	4.74 E+20	3.67 E+20
500	1.25 E+17	1.27 E+17	9.67 E+16
600	4.84 E+14	4.97 E+14	3.75 E+14
700	8.80 E+12	9.09 E+12	6.83 E+12
800	4.21 E+11	4.38 E+11	3.28 E+11
900	3.87 E+10	3.96 E+10	3.02 E+10
1,000	5.62 E+09	5.89 E+09	4.40 E+09
1,500	1.49 E+07	1.58 E+07	1.17 E+07
2,000	6.79 E+05	7.29 E+05	5.34 E+05
2,500	1.00 E+05	1.08 E+05	7.85 E+04

[a] CVT/μOMT values

[b] Ref. [6]

[c] CVT/μOMT values on the PES-2005, Ref. [1]

experimental data, an improvement over PES-2005. This is an interesting result because the equilibrium constants permit one to obtain the reverse rate constants, which have yet to be measured experimentally.

4.3 Dynamics study

Reaction cross-sections, σ_R/Å². The QCT results on the PES-2010 surface are listed in Table 7 for the collision energy of 15.0 kcal mol⁻¹, using the different counting

Table 7 Reaction cross-sections, σ_R/Å², at 15.0 kcal mol⁻¹ for the H + CCl₄ reaction using the PES-2010

Counting method	σ_R/Å²
N_r^{all}/N_T	2.45 (2.60)
$N_r^{HB\text{-}DZPE}/N_T$	2.44 (2.10)
N_r^{all}/N_T'	3.37
$N_r^{HB\text{-}DZPE}/N_T'$	3.36

In parentheses, values with the PES-2005

Maximum error bar: ±0.01

methods: N_r^{all}/N_T; $N_r^{HB\text{-}DZPE}/N_T$; N_r^{all}/N_T'; $N_r^{HB\text{-}DZPE}/N_T'$. As expected, the results are sensitive to the ZPE criterion used, although comparatively less than in typical hydrogen abstraction reactions [42] due to the lower values of the ZPEs of both products, CCl_3 and HCl. However, removing the non-reactive trajectories that do not fulfill the ZPE criterion (using N_T') has a significant influence on the results, multiplying the reaction cross-section by a factor of 1.4. Unfortunately, neither theoretical nor experimental data on the dynamics of this reaction are available, but for the hydrogen abstraction reaction, $H + NH_3$ [42], we showed that the last counting method, $N_r^{HB\text{-}ZPE\text{-}HCl}/N_T'$, reproduces the QM results best [43]. This analysis illustrates the importance of avoiding criteria based on individual trajectories, because quantum mechanical constraints apply to ensembles [38]. Finally, the PES-2005 results are also listed in Table 7, and one observes that, when the same counting method is used, the cross-sections from the two surfaces agree well.

Product energy partitioning. Table 8 lists the QCT average product fraction of energy in translation, f'_{trans}, and in vibration and rotation of HCl and CCl_3, $f'_{vib}(HCl)$, $f'_{rot}(HCl)$, $f'_{vib}(CCl_3)$, and $f'_{rot}(CCl_3)$, at 15.0 kcal mol^{-1}, together with the theoretical values from PES-2005 for comparison. For PES-2010, about 40% of the energy ends up in translational energy, while the HCl product and the CCl_3 co-product appear with moderate and similar amounts of internal energy, ≈ 27–30% of the total available energy. The collinear character of the transition state explains the low rotational excitation of the products (4 and 2%, respectively), and the high proportion of translational energy. The PES-2005 description is very different. Thus, only 23% of the energy ends up in translational energy, with the largest portion (about 60%) in vibrational energy of the CCl_3 co-product. These differences are due to the different topology of the two surfaces, which, as was noted above, has a clear influence of the product energy partitioning, with the earlier surface overestimating the CCl_3 contribution, and underestimating the HCl product contribution.

To test the influence of the zero-point energy correction on this property, calculations considering all trajectories were also performed, i.e., without removing the trajectories with energies below the ZPE of the products. The results are also listed in Table 8. As noted above, in this particular reaction, the influence of the ZPE criterion chosen is small or negligible, due to the small values of the ZPEs in both products, CCl_3 and HCl.

HCl(v', j') product vibrational and rotational distributions. The HCl(v') vibrational distributions calculated with the QCT method using both the PES-2010 and the PES-2005 surfaces are plotted in Fig. 4, where the vibrational number is rounded to its nearest integer part. The two

Table 8 Product energy partitioning (percentages) for the H + CCl$_4$ reaction at 15.0 kcal mol^{-1}

| Reference	f_{trans}	$f_{vib}(HCl)$	$f_{rot}(HCl)$	$f_{vib}(CCl_3)$	$f_{rot}(CCl_3)$
This work, PES-2010					
No-ZPE	42	23	4	29	2
HB-DZPE	42	23	4	29	2
PES-2005					
No-ZPE	23	9	4	63	1
HB-DZPE	22	12	4	61	1

Maximum error bar calculated in this work, ± 1
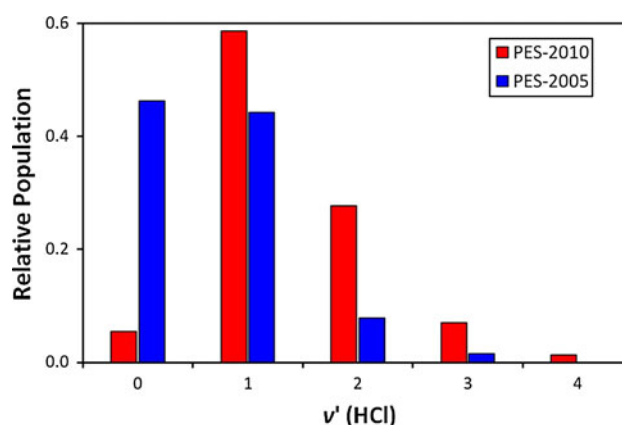

Fig. 4 Vibrational population for the HCl(v') co-product in the H + CCl$_4$ reaction at 15.0 kcal mol^{-1}, using the PES-2010 (*red*) and PES-2005 (*blue*) surfaces

surfaces give very different descriptions of this property, with the PES-2010 surface giving a larger vibrational excitation of the HCl co-product, related with its greater available vibrational energy, 23% of the total energy, versus 12% for PES-2005. With PES-2010, there is an inversion of the vibrational population, with a peak for $v' = 1$ (59%). This result confirms the qualitative predictions of the reaction path analysis (Sect. 4.1; Fig. 2) on the vibrational excitation of the HCl product, and highlights the capacity of this analysis in the qualitative dynamics description, especially useful in polyatomic reactions.

The QCT state-resolved HCl(v') rotational distributions using PES-2010 are plotted in Fig. 5. This surface reproduces the universal behavior for direct bimolecular reactions, i.e., the higher the vibrational state, the colder the rotational distribution. The rotational distributions are broad, especially at low vibrational levels, reaching up to $j' = 16$ at $v' = 0$. In general, this behavior has been described as an artifact of the QCT methods [44–50], due to its classical nature, and when theoretical quantum–
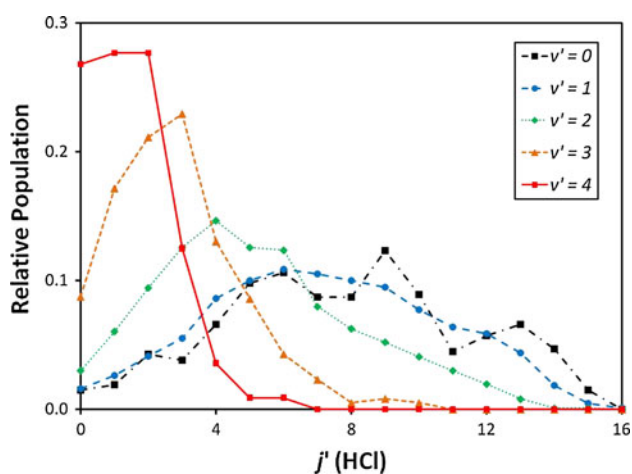
Fig. 5 Vibrational state-resolved rotational populations for the HCl product in the H + CCl$_4$ → HCl (v', j') + CCl$_3$ reaction
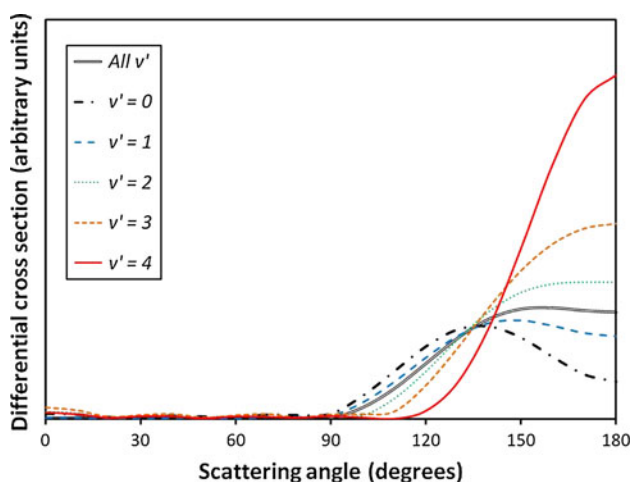
Fig. 6 Vibrational state-resolved product angular distributions for the H + CCl$_4$ → HCl (v', j') + CCl$_3$ reaction. The areas under the curves are normalized

mechanical calculations are performed, one must expect narrower and colder rotational distributions. However, in this particular case, the quantum effects (ZPE corrections to the trajectories and tunneling corrections) are practically negligible, and so the QCT method is suitable in this case.

Differential cross-section. This property is doubtless one of the most sensitive dynamics features with which to test the quality of the potential energy surface. The QCT vibrationally state-resolved HCl(v') scattering angular distributions on PES-2010 at a collision energy of 15.0 kcal mol^{-1} are plotted in Fig. 6. All the vibrational states show backward scattering, and as the vibrational state increases, HCl($v' = 0 \rightarrow v' = 4$), the scattering becomes increasingly backwards oriented. This is the

expected behavior for a rebound mechanism with low impact parameters, and it is favoured by the collinear configuration of the transition state. The PES-2005 presents the same behavior, with backward scattering, and is therefore not represented here.

5 Comparison of the H + Cl$_2$ and H + CCl$_4$ reactions

As has been noted throughout the text, no experimental dynamics data are available for the title reaction, so that we shall use a comparison with the well-studied and similar L + HH mass combination H + Cl$_2$ reaction to try to shed some light on the present results. Indeed, the H + Cl$_2$ reaction has received much experimental attention, and several of its properties have been determined: HCl vibrational and rotational distributions [51–55], DCS scattering distributions in the D + Cl$_2$ reaction [56], and thermal rate constants [57, 58]. Table 9 summarizes some important features of the two reactions.

The barrier heights follow Hammond's postulate, i.e., the higher the exothermicity, the lower the barrier. Due to the similar light-heavy-heavy (LHH) mass combination, the skew angle, β, between the axes of the entrance and exit valleys of the potential energy surface is close to $\pi/2$ in both reactions. Under these conditions, the typical trajectory is practically rectilinear, where the H atom approaches

Table 9 Some energy and dynamics properties for the H + Cl$_2$ and H + CCl$_4$ reactions

	H + Cl$_2$	H + CCl$_4$
Energy		
$\Delta H_R(0\ K)$	−45.2	−32.1
$\Delta E^{\neq}$	0.55	5.4
Skew angle	83°	82°
Product energy partitioning		
f_{trans}	0.53	0.42^a
f_v(HCl)	0.39 ± 0.03	0.23
f_r(HCl)	0.08 ± 0.01	0.04
f_v(CCl$_3$)		0.29
f_r(CCl$_3$)		0.02
HCl(v') *vibrational population*		
$v' = 0$		0.05
$v' = 1$	0.14 ± 0.03	0.59
$v' = 2$	0.40 ± 0.04	0.28
$v' = 3$	0.40 ± 0.04	0.07
$v' = 4$	0.05 ± 0.01	0.01
Differential cross-section	Backward, 180°	Backward, 180°

$\Delta H_R(0\ K)$, enthalpy of reaction at 0 K; $\Delta E^{\neq}$, classical barrier height, both in kcal mol^{-1}

^{a} Maximum error bar calculated in this work, ±0.01

closely before Cl–C repulsion sets in and abruptly accelerates the separation of the co-product (Cl or CCl_3, respectively), leading to the products having a major translational energy. Simultaneously, the energy released as rotation is small (4–8% of the total energy), and the HCl product will therefore appear rotationally cold. This is due to the collinear character of the transition state and to the fact that the center-of-mass of the HCl molecule is practically in the chlorine atom. As for the $HCl(v')$ vibrational distribution, both reactions present population inversion, i.e., they are potential chemical lasers, peaking at $v' = 2$–3 and $v' = 1$ for the $H + Cl_2$ and $H + CCl_4$ reactions, respectively. This difference can be explained by the higher available energy in the case of the $H + Cl_2$ reaction. Note that this behavior differs from that observed with the previous PES-2005 which predicts no vibrational population inversion. Finally, both reactions present a similar reaction mechanism—a direct bimolecular reaction, associated with a rebound mechanism with low impact parameters.

6 Conclusions

In this work, we have reformulated and recalibrated a previous analytical potential energy surface for the gas-phase $H + CCl_4 \rightarrow HCl(v', j') + CCl_3$ reaction. The new surface, named PES-2010, is more flexible than the previous PES-2005, and the calibration is now also intended to reproduce the topology of the reaction path from reactants to products, i.e., the calibration performed was not limited to the saddle point zone. Moreover, the input information used for the fit was exclusively based on electronic structure calculations, and no experimental data was used, avoiding the semiempirical character of the previous PES.

First, a kinetics study using variational transition-state theory (VTST) with multidimensional tunneling was performed over the temperature range 300–2,500 K. The thermal forward rate constants agreed with the experimental information in the common temperature range, taking into account the experimental error bar, improving previous theoretical results from other groups. Due to it being the heavy chlorine atom which is tunneled, the transmission coefficient is small. The equilibrium constants, which depend only on reactant and product properties, agree with experiment. This information, although macroscopic, can be useful in dynamics analyses, because it is a good test of the accuracy of their description. The analysis of the reaction path curvature (kappa factor) showed qualitatively that large H–Cl stretching vibrational excitation is expected in the products. This qualitative prediction agrees with the quantitative dynamics results of the present work.

Second, an exhaustive dynamics study employing quasi-classical trajectory (QCT) calculations was also performed on this PES-2010. The product energy partition obtained shows that the energy released into product translation is high (about 40%), where the $HCl(v', j')$ product appears with low rotational energy and vibrational population inversion, peaking at $v' = 1$. The product angular distribution appears clearly in the backward hemisphere, indicating a rebound mechanism associated with low impact parameters.

Third, unfortunately no experimental data are available for the title reaction, but the comparison with the similar and experimentally well-studied $H + Cl_2$ reaction showed similar dynamics and mechanism patterns, indirectly supporting our dynamics results.

In accordance with the goals set out in the Introduction, the PES-2010 improves the results of the earlier PES-2005 since it better reproduces the electronic structure reaction path, giving a deeper fall in energy in the product valley. This behavior has a direct consequence on the dynamics description of the reaction.

In sum, the agreement obtained using the newly constructed surface with the available kinetics measurements, and with the dynamics results of the similar light-heavy-heavy $H + Cl_2$ reaction, lends confidence to the new PES-2010 surface.

Finally, the fact that ZPE corrections to the trajectories and tunneling corrections to the reaction rates are relatively small, both being quantum effects, leads us to think that this reaction behaves in a classical way. We have to take into account that because of the masses of the atoms involved, the energy levels are closely spaced and energy levels can be approximately taken as a continuum of energy. Therefore, one would expect the present QCT methods to be more accurate than when applied to lighter systems, where quantum effects are much more important and they can control the reactivity of the system.

References

1. Rangel C, Espinosa-Garcia J (2005) J Chem Phys 112:134315
2. Bryukov MG, Slagle IR, Knyazev VD (2001) J Phys Chem A 105:3107
3. Knyazev VD (2002) J Phys Chem A 106:11603
4. Sheng L, Li Z-S, Liu J-Y, Xiao JF, Sun C-C (2002) J Phys Chem A 106:12292
5. Louis F, Gonzalez CA, Sawerysyn JP (2004) J Phys Chem. A 108:10586
6. JANAF Thermochemical Tables (1985). In: Chase MW Jr, Davies, CA, Downey JR, Frurip DJ, McDonald RA, Syverud AN (eds) National Bureau of Standards, Washington, DC, vol 14, 3rd edn

7. Pu J, Truhlar DG (2002) J Chem Phys 116:1468
8. London F (1928) Problema der modernen Physik (Sommerfeld Festschrift) p 104; Eyring H, Polanyi M (1931) Z Phys Chem 1312:279
9. Chakraborty A, Zao Y, Lin H, Truhlar DG (2006) J Chem Phys 124:044315
10. Jordan MJT, Gilbert RG (1995) J Chem Phys 102:5669
11. Isaacson TruhlarDG, AD GarrettBC (1985) In: Baer M (ed) Theory of chemical reaction dynamics, vol 4. Chemical Rubber, Boca Raton, p 65
12. Fast PL, Truhlar DG (1998) J Chem Phys 109:3721
13. Jackels CF, Gu Z, Truhlar DG (1995) J Chem Phys 102:3188
14. Chuang Y-Y, Truhlar DG (1998) J Phys Chem A 102:242
15. Miller WH, Handy NC, Adams JE (1980) J Chem Phys 72:99
16. Morokuma K, Kato S (1981) In: Truhlar DG (ed) Potential energy surfaces and dynamics calculations. Plenum, New York, p 243
17. Kraka E, Dunning TH (1990). In: Advances in molecular electronic structure theory. JAI, New York, vol I, p 129
18. Garrett BC, Truhlar DG, Grev RS, Magnuson AW (1980) J Phys Chem 84:1730 (1983) 87: 4554(E)
19. Liu Y-P, Lynch GC, Truong TN, Liu D-H, Truhlar DG (1993) J Am Chem Soc 115:2408
20. Truong TN, Lu D-H, Lynch GC, Liu Y-P, Melissas VS, Stewart JJ, Steckler R, Garrett BC, Isaacson AD, González-Lafont A, Rai SN, Hancock GC, Joseph T, Truhlar DG (1993) Comput Phys Commun 75:43
21. Meana-Pañeda R, Truhlar DG, Fernandez-Ramos A (2010) J Chem Theor Comp 6:6
22. Corchado JC, Chuang Y-Y, Fast PL, Villa J, Hu W-P, Liu Y-P, Lynch GC, Nguyen KA, Jackels CF, Melissas VS, Lynch BJ, Rossi I, Coitiño EL, Fernández-Ramos A, Steckler R, Garrett BC, Isaacson AD, Truhlar DG (2000) POLYRATE, version 8.5.1. University of Minnesota, Minneapolis
23. Porter RN, Raff LM (1976) In: Miller WH (ed) Dynamics of molecular collisions, part B. Plenum Press, New York
24. Truhlar DG, Muckerman JT (1979) In: Bernstein RB (ed) Atom-molecules collision theory. Plenum Press, New York
25. Raff LM, Thompson DL (1985) In: Baer M (ed) Theory of chemical reaction dynamics, vol 3. CRC Press, Boca Raton
26. Hase WL, Duchovic RJ, Hu X, Komornicki A, Lim KF, Lu D-H, Peslherbe GH, Swamy KN, Van de Linde SR, Varandas AJC, Wang H, Wolf RJ (1996) VENUS96: a general chemical dynamics computer program. QCPE Bull 16:43
27. Rangel C, Corchado JC, Espinosa-Garcia J (2006) J Phys Chem A 110:10375
28. Bowman JM, Kuppermann A (1973) J Chem Phys 59:6524
29. Truhlar DG (1979) J Phys Chem 83:18
30. Schatz GC (1983) J Chem Phys 79:5386
31. Lu D-H, Hase WL (1988) J Chem Phys 89:6723
32. Varandas AJC (1994) Chem Phys Lett 225:18
33. Ben-Nun M, Levine RD (1996) J Chem Phys 105:8136
34. McCormack DA, Lim KF (1999) Phys Chem Chem Phys 1:1
35. Stock G, Müller U (1997) J Chem Phys 111:65
36. Marques JMC, Martinez-Nuñez E, Fernandez-Ramos A, Vazquez S (2005) J Phys Chem 109:5415
37. Duchovic RJ, Parker MA (2005) J Phys Chem 109:5883
38. Guo Y, Thomson DL, Sewell TD (1996) J Chem Phys 104:576
39. Kudla K, Schatz GC (1993) Chem Phys 175:71
40. Bethardy GA, Wagner AF, Schatz GC, ter Horst MA (1997) J Chem Phys 106:6001
41. Bonnet L (2008) J Chem Phys 128:044109
42. Espinosa-Garcia J, Corchado JC (2010) J Phys Chem A
43. Yang M, Corchado JC (2007) J Chem Phys 126:214312
44. Gerrity DP, Valentini JJ (1984) J Chem Phys 81:1298
45. Kliner DAV, Rinnen KD, Zare RN (1990) Chem Phys Lett 166:107
46. Bean BD, Fernandez-Alonso F, Zare RN (2001) J Phys Chem A 105:2228
47. Bean BD, Ayers JD, Fernandez-Alonso F, Zare RN (2002) J Chem Phys 116:6634
48. Bañares L, Aoiz FJ, Honvault P, Bussery-Honvault B, Launay JM (2003) J Chem Phys 118:565
49. Pomerantz AE, Ausfelder F, Zare RN, Althorpe SC, Aoiz FJ, Bañares L, Castillo JF (2004) J Chem Phys 120:3244
50. Xie T, Bowman JM, Duff JW, Braunstein M, Ramachandran B (2005) J Chem Phys 122:014301
51. Anlauf KG, Horne DS, Macdonald RG, Polanyi JC, Woodall KB (1972) J Chem Phys 57:1561
52. Ding AMG, Kirch LJ, Perry DS, Polanyi JC, Schreiber JL (1973) Faraday Discuss Chem Soc 55:252
53. Wickramaaratchi MA, Setser DW, Hilderbrant B, Korbitzer B, Heydtmann H (1984) Chem Phys 84:105
54. Hilderbrant B, Vanni H, Heydtmann H (1984) Chem Phys 84:125
55. Berg PA, Sloan JJ (1994) J Chem Phys 100:1075
56. Mcdonald JD, LeBreton PR, Lee YT, Herschbach DR (1972) J Chem Phys 56:769
57. HGg Wagner, Welzbacher U, Zellner R (1976) Ber Bunsenges Phys Chem 80:902
58. Bemand PP, Clyne MAA (1977) J Chem Soc Faraday Trans II 73:394